An In-depth Study of Energy-dispersive X-Ray Spectra

P. Van Espen, H. Nullens and F. Adams
Department of Chemistry, University of Antwerp (UIA), Universiteitsplein 1, B-2610 Wilrijk, Belgium

A detailed study of energy-dispersive X-ray spectra is undertaken. Considerable attention is given to a method for a systematic and accurate description of the K and L spectra; a digital correction for the peak profile is evaluated. The following second order effects and spectral artefacts are investigated: radiative Auger transitions, spectral background components, Raman scattering of X-rays, silicon escape, fluorescence of the detector materials, and sum peaks.

INTRODUCTION

Energy-dispersive X-ray emission spectrometry has become an attractive and widely used method for multielement analysis, particularly in the environmental field. Particle induced X-ray emission (PIXE) and tube-excited X-ray fluorescence (XES) provide a sufficient sensitivity for the determination of 10–20 elements in thin environmental samples as, for instance, air particulate material collected on filter paper. The attractive features of these techniques, compared to other analytical methods, are the multi-element character with a coverage of most of the environmentally important elements (except cadmium), the rapidity of the determination, and the non-destructive and easily automated analysis.

An important drawback of the method is the extreme density of spectral components in a rather limited energy range which necessitates a computer based data analysis by least-squares techniques.[1–3] These methods need a highly accurate description of all spectral components as a prerequisite. A detailed study reveals a considerable number of second order phenomena. It is the aim of this work to study X-ray spectra in detail, in order to overcome most of the problems encountered in the use of least-squares fitting for the analysis of the spectrum and to avoid analytical misinterpretation of the spectral data; attention is therefore focused on spectral artefacts and second order effects.

INSTRUMENTATION

Spectra were obtained with an X-ray spectrometer consisting of: a Kevex 810 excitation system with a high power tungsten anode X-ray tube, a secondary target + filter assembly which provides the possibility of using Ti, Ge, Mo, Ag, Sn and Nd K radiation, a collimated 30 mm^2 x 3 mm Kevex Si(Li) detector of 160 eV FWHM resolution at 5.895 keV, associated electronics for signal processing, and a conventional multichannel analyser for data acquisition.

Spectrum analysis is performed with a computer program, AXIL, which is based on non-linear least-squares fitting. The computer analysis has been described in detail elsewhere.[3]

THE CHARACTERISTIC X-RAY SPECTRUM

Fundamental

The radiative transition of an atom from a state A to a state B gives rise to a spectral distribution

$$I_0(E) \sim \frac{1}{\pi} \frac{\Gamma/2}{(E_0 - E)^2 + (\Gamma/2)^2} \tag{1}$$

where E_0 is the mean energy of the transition. For the line width, the following relations hold:

$$\Gamma = \Gamma_A + \Gamma_B \tag{2}$$

$$\Gamma_A = \Gamma_{A,\text{radiative}} + \Gamma_{A,\text{Auger}} \tag{3}$$

Equation (1) is the well known Lorentz distribution. Typically, the total energy broadening is less than 4 eV for the K state and 2–3 eV for the L_2 and L_3 states of elements with atomic number below 50;[4] the Lorentz width is of the order of 10 eV.

Peak profiles measured with semiconductor detectors are a convolution of the Lorentz distribution with the response function of the detection system, $D(E)$:

$$I(E) \sim \int_{-\infty}^{+\infty} I_0(E') D(E - E')\, dE' \tag{4}$$

$D(E)$ is generally assumed to be a Gaussian and the fluorescence lines then correspond to a Voigt profile.[5] As the Lorentz width is much smaller than the width of the Gaussian response function, a Gauss function is an adequate first order representation of the peak profile.

The observed K emission spectrum of an element is the result of a transition between the K state and different higher energy states (L, M, N). Figure 1(a) represents the theoretically expected emission spectrum of sulphur, manganese and silver, calculated using the transition probabilities given by Scofield[6] and assuming an ideal Gaussian response function. It appears that three groups of transitions are of importance, namely: K–L_2L_3, K–M_2M_3 and K–N_2N_3. The question arises whether to represent these doublets in the non-linear least-squares fitting by a single Gaussian

CCC-0049-8246/80/0009-0126 $04.00

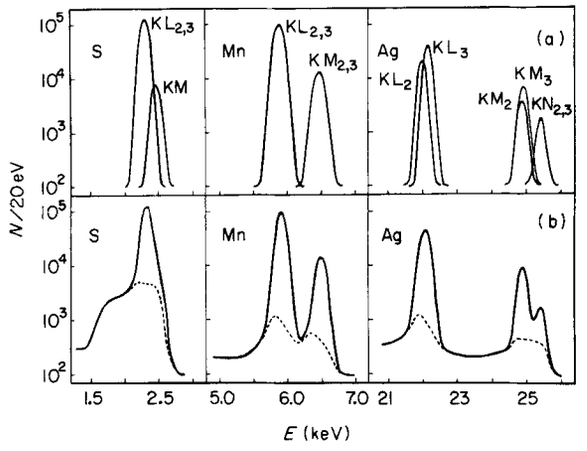

Figure 1. Theoretically expected X-ray emission spectrum (a) and systematic deviation from Gaussian peak shape (b) for sulphur, manganese and silver.

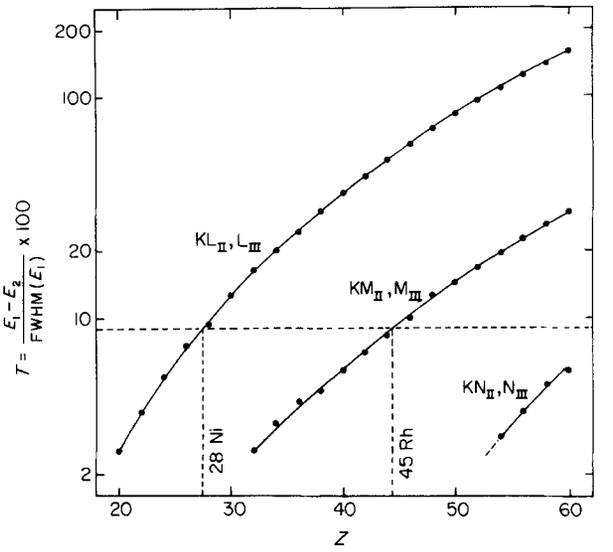

Figure 3. T versus atomic number for K lines.

or by two Gaussians. The answer, of course, depends on the energy resolution of the spectrometer and the precision with which it can be measured. It appears that, for high intensity peaks with a width of 200 eV FWHM, a width estimate cannot be made at better than 1 eV and hence one can assume that differences in peak width of less than 0.5% resulting from doublets are undetectable. To quantify the problem, the $K\alpha_{1,2}$ doublets of the elements chromium to zirconium were fitted with a single Gaussian (FWHM $K\bar{\alpha}$ and with two Gaussians (FWHM $K\alpha_1$ and $K\alpha_2$) using the energy difference and intensity ratio between $K\alpha_1$ and $K\alpha_2$. The percentage relative difference in observed peak width is plotted against a factor T which represents the energy difference between the peaks in the doublets, relative to the spectrometer resolution at this energy. It is apparent from Fig. 2 that a critical T value of 9 is obtained for the spectrometer used in this work. For values of T above this limit the doublet should be represented by the individual features; for values below 9, the representation by a single Gaussian is adequate.

Figure 3 represents T as a function of the atomic number for the three K doublets. The $K\alpha_{1,2}$ doublet has to be represented by two Gaussians starting from nickel, whereas this has to be done for the $K\beta_{1,3}$ doublet starting from rhodium. The $K\beta_{2,2'}$ doublet can be represented by a single Gaussian up to neodymium.

Although the criterion developed here is strictly speaking only applicable for doublets having an intensity ratio of 1 : 2, as is the case for the K doublets, the same approach can be used for L spectra. The L line spectra consist of three groups of transitions: for the L_1 group the doublets $L_1M_{3,2}$, $L_1N_{3,2}$, $L_1O_{3,2}$, $L_1M_{5,4}$ and $L_1N_{5,4}$ can be distinguished; the L_2 groups consists (in descending order of importance) of the lines L_2M_4, L_2N_4, L_2M_1, L_2N_1, L_2O_4 and L_2O_1; the L_3 transitions have the doublets $L_3M_{5,4}$, $L_3N_{5,4}$, $L_3O_{5,4}$ and the lines L_3N_1 and L_3O_1. This is a total of 24 transitions among which 16 have a double structure. In Fig. 4 the T value for these doublets is represented for the different elements. Again it can be decided easily and unambiguously which doublets have to be represented by two Gaussians.

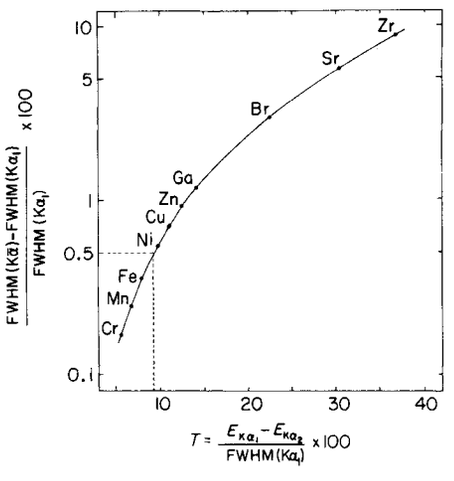

Figure 2. Relative difference in energy resolution of single Gaussian with energy $E_{K\bar{\alpha}}$ and doublet with $E_{K\bar{\alpha}_1}$ and $E_{K\bar{\alpha}_2}$ plotted against T.

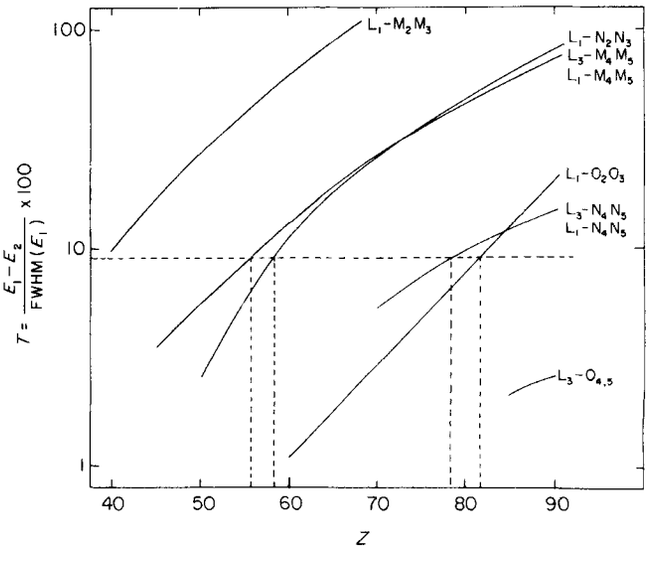

Figure 4. T versus atomic number for L lines.

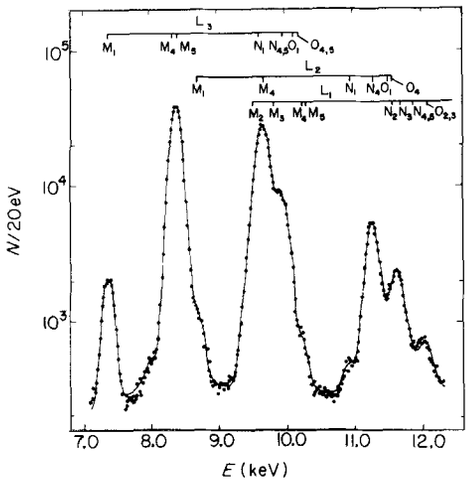

Figure 5. Fit through tungsten L spectrum.

The exploitation of the strategy of doublet representation is illustrated in Fig. 5, where an observed and a fitted tungsten L spectrum are shown. Constant intensity ratios, calculated from the work of Scofield,[7] were used between the two peaks in the doublets. The intensity ratios between different lines of the same L group, as determined by the fit, are in good agreement with literature data.[8]

The peak profile

Assuming spectral peaks to be Gaussian may lead to errors in the deconvolution of multiplets, however. Accurate determinations with an energy-dispersive spectrometer thus require a closer description of the instrumental response. The problem has been dealt with often for the case of high resolution gamma-ray spectra obtained with Ge(Li) detectors. A number of analytical functional descriptions of the full energy peaks have been proposed. A review of these has been given by Mc Nelles and Campbell[9] who also investigated the problem for the description of low energy peaks from Si(Li) detectors. These methods invariably require a large number of parameters for the description of a single peak and this complicates enormously the computer analysis of the spectrum. We therefore preferred a method which introduces no extra parameters in the calculation. It relies on the determination and the use of the difference between the measured response function and the Gauss function as a numerically stored correction $C(i)$. A detailed description of this method for the accurate description of the full energy peaks is given in an earlier publication.[10]

Figure 1(b) shows the experimentally observed fluorescence spectra of sulphur excited with titanium primary radiation, of manganese excited with molybdenum, and of silver excited with neodymium. The dashed line is obtained by subtracting the Gaussian response from the observed spectra. The method used to perform this is described in detail elsewhere.[10]

It appears immediately that the deviation from the Gaussian peak shape is of the order of a few percent and that its shape depends on the energy of the lines. It seems logical to suspect the detector to be the cause of the non-Gaussian part of the spectrum. That the detection system cannot be solely responsible for it is suggested by the form of the manganese spectrum shown in Fig. 1(b). In fact, the non-Gaussian part associated with the Mn Kβ component is proportionally more intense that that of Mn Kα. Both lines differ by less than 600 eV in energy and one might assume that the detector response for both lines is quite nearly identical. This suggests that a portion of the non-Gaussian component of the spectrum originates in the sample and has a radiative nature.

In order to investigate the different components of the non-Gaussian part of the spectrum a number of experiments were carried out.[11] Every point $C_0(i)$ in the correction set for the K radiation of an element can be considered as originating from sample effects, $X(i)$, i.e. emitted radiation different from the discrete spectrum lines on the one hand, and from detector effects, $D(i)$, i.e. non-Gaussian detector response, for the main lines on the other hand. For simple K line spectra this becomes

$$C_0(i) = X(i) + D_{K\bar{\alpha}}(i) + D_{K\bar{\beta}}(i) \qquad (5)$$

taking K$\bar{\alpha}$ and K$\bar{\beta}$ as single spectral components for simplicity. One or more of these components can be wholly or partially removed from the spectrum by placing a suitable absorbing filter, j, in front of the detector, i.e. a set of equations

$$C_j(i) = \exp[-\mu_j(E_i)\rho_j d_j]\, X(i) + \exp[-\mu_j(E_{K\bar{\alpha}})\rho_j d_j] \times D_{K\bar{\alpha}}(i) + \exp[-\mu_j(E_{K\bar{\beta}})\rho_j d_j]\, D_{K\bar{\beta}}(i) \qquad (6)$$

can be obtained and solved mathematically.

In the vicinity of the peaks, the solution of these equations will be subject to large uncertainties but, taking into account the close resemblance that must exist between the Kα and Kβ response, a reliable estimate for the values of the different component can be made. Figure 6, where the dashed lines indicate regions of low precision, shows the non-Gaussian components for the tin K spectrum obtained in this manner; absorbers used in this case were indium, silver and nickel. It can be seen that, at energies lower than Kα, most of the non-Gaussian part is due to the detector effects, while the 'radiative component' X is more important in the region between Kα and Kβ.

The physical origin of the radiative component is unclear. The Lorentz line profile could contribute significantly to it. In fact, the Lorentz contribution could become a dominant

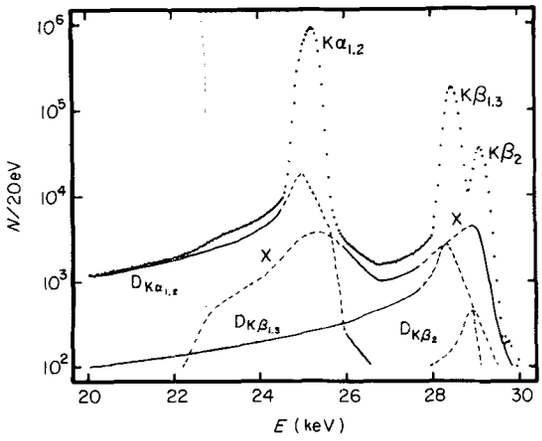

Figure 6. Deviation from Gaussian peak shape for tin K spectrum; contributing factors of Eqn (5), dotted line indicates regions of low precision.

factor over the Gaussian at a considerable distance from the peak maxima. The asymmetric behaviour of the radiative component indicates that the Lorentz form of the line is not the sole cause. Secondary effects associated with the atomic rearrangement after the creation of a K vacancy could give rise to a number of satellite-lines which do not become resolved with the limited energy resolution of the system.

The detailed analysis of the different components of the residual non-Gaussian part of the peak response is not possible for elements with low atomic number, as the energy difference between Kα and Kβ becomes too small to be able to determine the radiative component with sufficient accuracy, although it remains qualitatively detectable for most of the first transition series elements. It is, however, quite possible to determine the total deviation from the Gaussian peak shape for every element of interest. These data can then be used as a library and included in non-linear least squares fitting procedures for spectrum analysis. A computer analysis based on this approach is described by Nullens *et al.*[11] It provides for the accurate analysis of even weak component in complicated spectra.

As there is a smooth variation with atomic number, interpolation can be applied to determine the residual spectrum of the lines of an element which has not been investigated. It appeared that a set of 10 spectra was sufficient for the K lines of all elements of importance in energy-dispersive X-ray fluorescence.

The radiative Auger effect

In K X-ray spectra of elements with atomic number between 20 and 30 it is possible to detect a structure with a rather poorly defined maximum and a slowly declining tail. This structure is shown in Fig. 7 for zinc. Absorption experiments, similar to those explained previously, indicate that the effect is indeed radiative, i.e. originates in the sample and not in the detector. A detail of the $X(i)$ component of zinc is also plotted in Fig. 7.

This structure has been detected previously during the study of the emission spectra of the elements Al, Si and S using a high resolution crystal spectrometer, and has been explained as originating through the K–LL radiative Auger transition.[12] This is an alternative decay mode of the K vacancy with simultaneous emission of a photon $\hbar\omega$ and an L electron. The energy of the 'Auger' photon is given by

$$\hbar\omega = E(\text{K–LL}) - E_{\text{kin}}(\text{L}) \qquad (7)$$

with $E_{\text{kin}}(\text{L})$ = kinetic energy of the emitted L electron and $E(\text{K–LL})$ = K–LL Auger transition energy.

The kinetic energy of the emitted electron varies between zero and $E(\text{K–LL})$, hence $\hbar\omega$ is continuous with a maximum value equal to $E(\text{K–LL})$ for $E_{\text{kin}}(\text{L}) = 0$.

Since the RA transition is a rearrangement process competitive to K X-ray emission, the RA intensity is a fixed fraction of the Kα line for a given element, irrespective of the excitation mode of the K vacancy.[13,14] The intensity of the RA band, relative to the Kα line, varies from approximately 1% for elements below calcium to less than 0.1% for elements above zinc. For chlorine and lower atomic number elements, the RA structure is not detectable with an Si(Li) spectrometer; due to the poor resolution the radiative Auger component overlaps completely with the Kα peak of these elements. The structure is most easily detectable for the elements titanium to zinc. For higher Z elements the RA effect becomes undetectable due to its low relative intensity. In most practical analytical situations, therefore, the RA effect will not cause any appreciable interference.

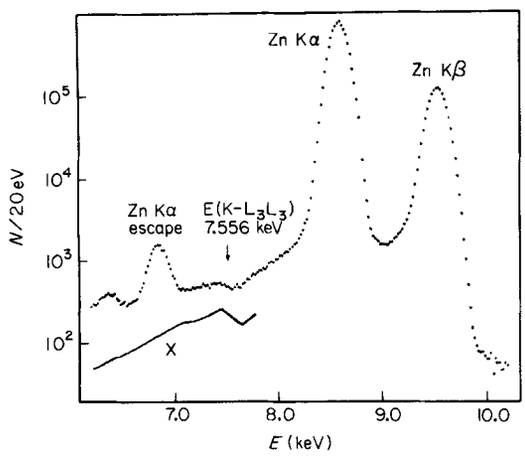

Figure 7. K spectrum of zinc with part of radiative or X-component.

BACKGROUND AND SCATTERED RADIATION

Spectral background

The background contribution of the ED X-ray spectrum is very important analytically. Most spectra are too complex to enable the determination of the background by direct interpolation between peaks. The background component results from several causes:[15]

bremsstrahlung of energetic photoelectrons in the sample;

the excitation radiation, if not monochromatic, may give rise to a scattered component of white radiation;

incomplete charge collection effects in the detector, mainly from the detection of the coherently and incoherently scattered monochromatic excitation radiation.

The first effect was studied in detail by Goulding;[16] it is most important at low energies, but of neglectable magnitude compared to the other background contributions. The background can hence be described entirely in terms of a contribution from the white tube spectrum and a contribution due to the detection of scattered monochromatic radiation.

The importance of the latter components for normal operating conditions of the spectrometer (Mo target, Mo filter, 40 kV and 40 mA) was estimated by comparing the spectrum from a 9 mg cm^{-2} cellulose matrix, taken in these conditions, with the spectra obtained after replacing the Mo target by a Ge and an Ag target. In this way the Mo K fluorescence from the target is absent while it can be assumed that the general shape of the scattered white tube spectrum is not substantially affected. In Fig. 8 the Mo K spectrum scattered on the cellulose sample is shown; the white radiation component (dashed line) becomes important from 10 keV upwards. Between 12 and 14 keV it amounts to nearly 50% of the total observed intensity. At

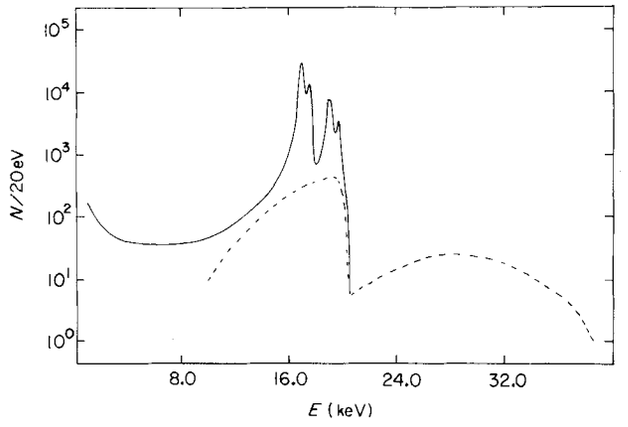

Figure 8. Mo K spectrum scattered from cellulose sample. Dotted line scattered primary radiation component of spectrum.

energies lower than 10 keV, incomplete charge collection of the scattered excitation radiation is the only background contribution of importance.

The background from an energy-dispersive secondary target X-ray spectrometer is thus mainly non-radiative in origin, and the shape is to a large extent independent of the sample being analysed. This opens several possibilities to describe the background for the entire spectrum.

A method has been described and verified in an earlier publication[17] to estimate the background at a particular energy, $B(E)$, from the number of counts in the incoherently and coherently scattered Mo Kα peaks:

$$B(E) = S(E)N_{K\alpha,\text{inc}} + R(E)N_{K\alpha,\text{coh}} \quad (8)$$

$S(E)$ and $R(E)$ are the proportionality factors for the incoherent and the coherent contribution respectively. The background description in the non-linear least squares fitting can be modelled by a function

$$B(E) = A_1 + A_2 \exp\left[\sum_{j=1}^{n} C_j(E - E_0)^j\right] \quad (9)$$

where E_0 is a suitable reference energy and A_j and C_j are parameters. Once optimized for a given set of spectra the C_j parameters are held constant, hence the complete background description requires only the estimation of the variable parameters A_1 and A_2. Sufficient accuracy is nevertheless retained. In Table 1 the observed background of a 9 mg cm^{-2} cellulose matrix (Mo K excitation 40 kV, 40 mA 3000 s in vacuum) is compared with that calculated using both methods described above. The agreement is satisfactory, with no significant differences between the observed and the calculated values.

Table 1. Comparison of the observed background (9 mg cm^{-2} cellulose matrix, Mo K excitation 3000 s, vacuum) with the calculated background

	Background (number of counts) in region of the element Kα line		
Element	Experimental	Using Eqn (8)	Using Eqn (9)
Cl	709 ± 27	–	706
K	679 ± 26	642	666
Ca	611 ± 25	609	631
Sc	527 ± 23	577	553
Ti	600 ± 24	579	595
V	554 ± 24	543	584
Cr	678 ± 26	677	636
Mn	647 ± 25	680	640
Fe	637 ± 25	657	660
Co	643 ± 25	643	616
Ni	705 ± 27	686	683
Cu	784 ± 28	750	793
Zn	839 ± 29	760	841
Ga	811 ± 28	887	833
Ge	1001 ± 32	1020	995
As	1159 ± 34	1270	1231
Se	1590 ± 40	1572	1529
Br	2069 ± 45	2027	1956
Rb	4073 ± 64	4114	3993
Sr	6227 ± 79	6098	6281
Y	10745 ± 104	–	10595

Scattering of the excitation radiation

The scattering of the excitation radiation on to the sample being analysed has a negative influence on the analytical performance of the spectrometer, since it causes most of the background observed in the spectrum. The intense incoherently and coherently scattered target radiation (Mo Kα, Mo Kβ) may, however, serve a useful analytical purpose. Since the incoherently scattered intensity and the coherently scattered intensity depend differently on the composition and the mass per unit area of the sample, it is possible to determine for samples of unknown composition the actual mass being analysed.[18] This allows the accurate determination of elements in non-uniform, irregularly shaped samples.

Apart from these very well-known scattering processes, it is possible to detect in spectra of some samples another kind of X-ray scattering. Raman scattering of X-rays has been predicted for a long time, but only conclusively proved to exist in 1959.[19] When an incident photon with energy E_0 ejects an electron from one of the inner shells of the atom, there is a possibility that only part of this energy is converted to kinetic energy of the outgoing electron. The remaining energy can be detected as a Raman photon with energy

$$E_{RA} = E_0 - E_{kin} - E_B \quad (10)$$

with E_{RA} = energy of the Raman photon; E_0 = incident photon energy; E_{kin} = kinetic energy of the ejected electron; E_B = binding energy of the electron.

Since the kinetic energy is not quantized, a band-like structure is observed with a maximum energy $E_0 - E_B$. The Raman effect is to be expected in analytical X-ray spectrometry, with the K radiation of element Z used for excitation, for elements having an atomic number $Z-2$ to $Z+7$.[20] In this case Raman scattering occurs on L electrons. For excitation energies between 15 and 25 keV Raman scattering on the K electrons of the elements aluminium to chlorine can also be observed.

Because of its high energy edge, the effect may appear as a peak in the spectrum with possible erronneous identification as a fluorescence line. The intensity of the Raman band increases as the incident photon energy comes closer to the binding energy of the electron. The observed intensity can amount to as much as 10% of the L fluorescence

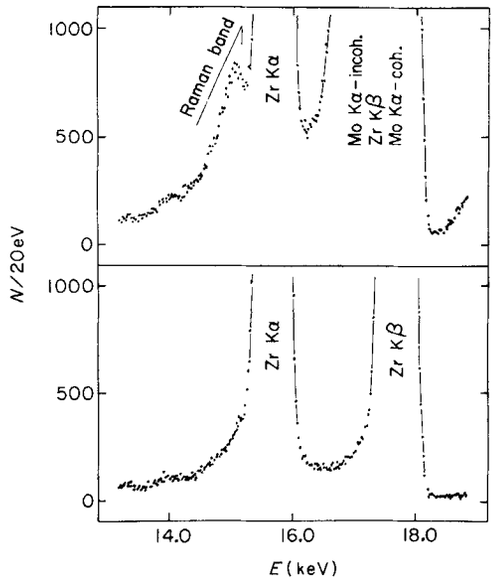

Figure 9. Zr K spectrum excited by Mo K radiation (top) and by Ag radiation (bottom).

intensity for excitation with Mo K X-rays of elements with atomic number between 45 and 48 in thick samples.

The phenomenon is of special importance in the spectrometer set-up used in this work. Indeed, a zirconium wire is suspended below the sample as a flux monitor,[21] so that Raman scattering is present in all spectra. Figure 9 illustrates this effect. The upper part represents the spectrum region of the Zr Kα, Kβ peak by excitation with Mo K X-rays; the lower part is obtained by irradiation with Ag K X-rays. The Raman band is clearly apparent in the case of Mo K excitation.

SECOND ORDER EFFECTS ASSOCIATED WITH THE DETECTION SYSTEM

A number of peak structures observed in the spectrum are due to artefacts in the detection system. Since they are not caused by interactions in the sample, they have no analytical use, but they can obscure the information content of the spectrum. Silicon escape peaks, the silicon internal fluorescence peak, gold and possibly tin fluorescence peaks are the result of interactions between the incident radiation and detector material; sum peaks and pile-up effects in general originate mainly in the electronic pulse processing circuit.

The silicon escape peak

Silicon escape gives rise to small but easily detectable satellite peaks in the spectrum. The effect is quite well known and results from the escape of Si K photons from the detector after photoelectric absorption of the detected X-rays in the edge regions of the detector.

The escape fraction f for photons with energy E is defined as the number of counts in the escape peak (N_e) over the number of detected counts ($N_m + N_e$). The escape fraction can be calculated rather easily for the case of X-ray spectrometry with collimated Si(Li) detectors if it is

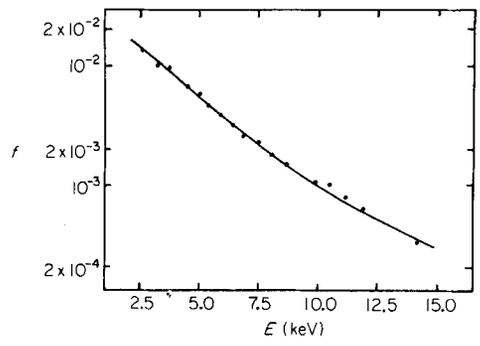

Figure 10. Si Kα escape function as a function of radiation energy; experimental data points and data calculated with Eqn (11).

assumed that the measured radiation is completely absorbed and hence escape occurs from the front surface of the detector only. For radiation penetrating the detector normal to its surface, the following formula can be derived:[22]

$$f_e = \frac{N_e}{N_m + N_e} = \frac{1}{2}\omega_K\left(1 - \frac{1}{r}\right)\left[1 - \frac{\mu_K}{\mu_I}\ln\left(1 + \frac{\mu_I}{\mu_K}\right)\right] \quad (11)$$

where μ_I and μ_K are the absorption coefficient of silicon for the impinging and the Si K radiation respectively; ω_K is the K fluorescence yield of silicon; and r is the K absorption jump ratio of silicon.

The calculated value for f using $\omega_K = 0.047$ and $r = 10.8$ is shown as a function of the radiation energy in Fig. 10 together with the experimentally determined values for the Kα radiation of the elements chlorine to strontium. It appears that the very simple model gives a quite accurate description of the escape fraction.

The position of the silicon escape is to be expected 1.742 keV (Si Kα) below the main peak. Careful analysis of highly intense spectra shows that the energy difference is slightly but significantly higher nml. 1.750 ± 0.002 keV. A possible explanation for this anomaly is that escape is more likely to occur in poorly compensated regions of the detector close to the surface where charge carrier losses are more important than in the bulk of the crystal. Table 2 shows the experimental data for a number of elements.

In view of the previous experimental fact it seemed worthwhile to ascertain whether the resolution of the escape peak is affected. It appeared that the FWHM of the K escape radiation is not significantly different from the spectrometer resolution at the energy of this peak. This is to be expected since the signal produced in the detector for an escape peak is the same as that produced by an

Table 2. Observed energy difference between main peak and escape peak for various Kα lines

Kα line	Energy difference (keV)
K Kα	1.747
Ti Kα	1.754
V Kα	1.749
Mn Kα	1.749
Fe Kα	1.750
Zn Kα	1.749
Average	1.750 ± 0.002

Table 3. Experimentally determined width of the escape peak, spectrometer resolution at the energy of the escape peak and width of the parent peak for various lines

	FWHM (eV)		
	Escape peak		
Kα line	Measured value	Spectrometer resolution	Parent peak
K Kα	135 ± 6	132	146
Ca Kα	138 ± 5	136	150
Fe Kα	164 ± 2	160	171
Co Kα	165 ± 2	164	178
Ni Kα	171 ± 2	169	181
Zn Kα	178 ± 5	178	191
Br Kα	200 ± 9	201	209
Sr Kα	213 ± 10	210	219

X-ray photon of the same energy. The escape peak is thus narrower than its parent. The relevant data are given in Table 3.

The silicon internal fluorescence peak

When the incident X-ray photon causes photoelectric interactions in the silicon deadlayer, the photoelectrons and the Auger electrons may be lost in the process of generating charge carriers. The emitted Si K photons, on the other hand, may enter the active region of the detector and produce a signal.

This Si K intensity relative to the incident radiation can be approximated for normal incident radiation by[23]

$$f_f = \frac{N_{SiK}}{N} = \frac{1}{2}\omega_K\left(1 - \frac{1}{r}\right)[\exp(-\mu_I d) - 1] \qquad (12)$$

where d is the thickness of the deadlayer and the other symbols are the same as in Eqn 10. For our detector we estimated by absorption measurements a deadlayer thickness of 0.3 μm. In this case f_f is ~ 0.5% for P Kα radiation, ~ 0.1% for Ca Kα and ~ 0.02% for Fe Kα radiation. It is very difficult to obtain experimental evidence for the validity of Eqn (11) since it is practically impossible to discriminate for an observed Si K peak between the Si K internal fluorescence contribution and the Si K fluorescence from traces of silicon present in the sample as a contamination.

Fluorescence of the detector materials.

Most Si(Li) detectors have a very thin gold layer on the entrance surface. For photons with energy in excess of the Au L absorption edge (L_I = 14.354, L_{II} = 13.736 and L_{III} = 11.921 keV), fluorescence is possible which gives rise to the detection of the Au L lines. It is possible to calculate the intensity of the Au L lines, relative to the intensity of the incident radiation.[24] The relative intensity of the Au $L\alpha_{1,2}$ peak is given by

$$f_{Au} = \frac{N_{AuL\alpha_{1,2}}}{N} = \frac{1}{2}\omega_3 f_{L\alpha}\rho_{Au} d_{Au}[\tau_1(f_{13} + f_{12}f_{23}) + \tau_2 f_{23} + \tau_3] \qquad (13)$$

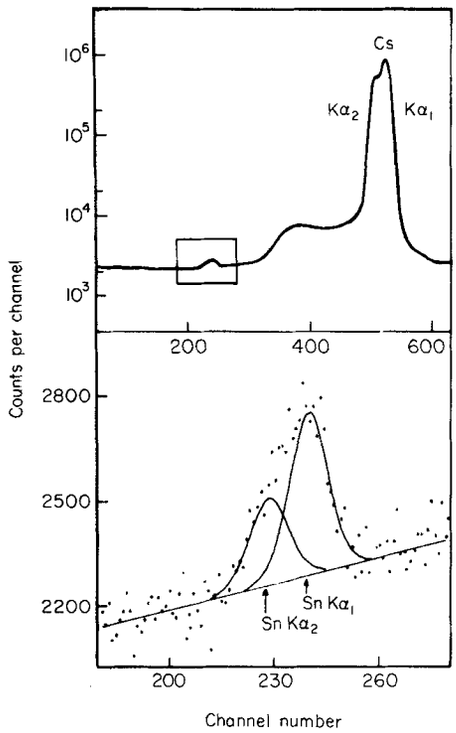

Figure 11. Cs K spectrum (^{133}Ba source) with Sn $K\alpha_1 - K\alpha_2$ fluorescence lines.

where ω_3 = Au L_3 fluorescence yield; $f_{L\alpha}$ = fraction of $L\alpha_{1,2}$ to all L_3 transitions; τ_i = L_i subshell photoelectric cross-section; f_{ij} = L_iL_j Coster–Kronig transition probability; ρ_{Au} = density of gold; d_{Au} = thickness of the gold contact.

In Eqn (12) it is assumed that half of the fluorescence photons generated reach the detector. The term between square brackets is the cross-section for formation of an L_3 subshell vacancy by direct excitation or by Coster–Kronig transitions. $\omega_3 f_{L\alpha}$ is the probability that this vacancy gives rise to a radiative process and Au Lα photon emission. With our equipment, using secondary target excitation, gold fluorescence is mostly due to the scattered Mo Kα,β radiation penetrating the detector. For a total of 34.8×10^6 photons detected, with a weighted average energy of 17.4 keV, we observed an Au $L\alpha_{1,2}$ peak of 11.5×10^3 counts. Using the physical constants from the literature[4,7,25] it can be deduced from Eqn (12) that the gold layer thickness is approximately 250 Å – close to the value of 200 Å which is generally stated by manufacturers. Knowing this thickness Eqn (12) can be used to subtract the Au L contribution of the detector Au layer from gold fluorescence in the sample. However, this is seldom necessary since it can be expected that gold is not present with a sufficient concentration in most samples. The presence in the spectrum of the Au Lα and Au Lβ lines has to be accounted for in the calculation, as it interferes with the spectrum deconvolution in the region between Ge Kα and Br Kα.

The detection of high energetic radiation (> 30 keV) with an Si(Li) detector can lead to the observation of Sn K lines in the spectrum, as a result of excitation of tin solder present close to the detector in the cryostat. Figure 11 shows the highly intense Cs spectrum from a ^{133}Ba-source and a detail of the energy region around 25 keV. The full

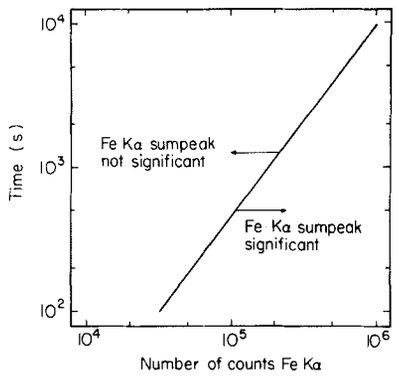

Figure 12. Region of significance of sumpeaks for iron Kα random summing.

lines are the result of a non-linear least-squares fit of the data with a straight line background and two Gaussians with intensity ratio 1 : 2.

Pile-up effects

With the use of pulse pile-up rejection networks in the detection electronics, random summing can be suppressed to a large extent, but never eliminated. With a well regulated rejection circuitry pile-up effects cause sumpeaks which can be corrected for easily. The count rate in a sumpeak is given by

$$\dot{N}_{S_{11}} = \tau \dot{N}_1 \dot{N}_1 \quad (14)$$

and

$$\dot{N}_{S_{12}} = 2\tau \dot{N}_1 \dot{N}_2 \quad (15)$$

where $\dot{N}_{S_{11}}$ = count rate in a sumpeak due to the pile-up of two pulses with the same energy; $\dot{N}_{S_{12}}$ = count rate in a sumpeak resulting from the coincidence of two different pulses; $\dot{N}_1$, $\dot{N}_2$ = count rate of the parent peak; τ = pulse pair resolution time.

As an example, Fig. 12 shows the conditions where the Fe Kα sumpeak becomes significant above the background in spectra obtained with Mo K excitation for a typical pulse pair resolution time of 3×10^{-6} s. It appears clearly that, even for normal analytical conditions, sumpeaks are to be expected in the spectrum and need to be accounted for. With the spectrometer used in this work, the sumpeaks are located very close to their expected position, with a deviation below 2 eV; they are approximately 5% wider than normal peaks located at the same position in the spectrum.

CONCLUSIONS

It is shown that a number of second order phenomena can obscure the analytical information in the energy-dispersive X-ray spectrum. Overlooking or ignoring these effects may result in erronneous assignment of spectral components to fluorescence peaks and cause problems for the least-squares deconvolution of the spectrum. Therefore, knowledge about the spectral shape, probability of occurrence and relative intensity of the fluorescence peaks, escape peaks and sumpeaks is necessary, and second order effects, such as the radiative Auger effects, Raman scattering and fluorescence of several detector materials, have to be recognized.

REFERENCES

1. H.C. Kaufmann, R. Akselsson and W.I. Courtney, *Nucl. Instrum. Methods* **142**, 142 (1977).
2. R.D. Wellis, *Nucl. Instrum. Methods* **142**, 231 (1977).
3. P. Van Espen, H. Nullens and F. Adams, *Nucl. Instrum. Methods* **142**, 243 (1977).
4. W. Bambynek, B. Crasemann, R.W. Fink, H.V. Freund, H. Mark, C.D. Swift, R.E. Price and P. Venugopala Rao, *Rev. Mod. Phy.* **44**, 716 (1972).
5. D.H. Wilkinson, *Nucl. Instrum. Methods* **95**, 259 (1971).
6. J.H. Scofield, *Phys. Rev.* **A9**, 1041 (1974).
7. J.H. Scofield, *Phys. Rev.* **A10**, 1507 (1974).
8. S.I. Salem, P.C. Clark and R.T. Tsutsui, *Phys. Rev.* **A5**, 2390 (1972).
9. L.A. Mc Nelles and J.L. Campbell, *Nucl. Instrum. Methods* **127**, 73 (1975).
10. P. Van Espen, H. Nullens and F. Adams, *Nucl. Instrum. Methods* **145**, 579 (1977).
11. H. Nullens, P. Van Espen and F. Adams, in *Proceedings of the Conference on Computers in Activation Analysis and Gamma-ray Spectroscopy CONF-780421*, edited by B.S. Carpenter, M.D. D'Agostino and H.P. Yule. Technical Information Center, US Department of Energy (1–4 May 1978).
12. T. Åberg and J. Utriainen, *Phys. Rev. Lett.* **22**, 1346 (1969).
13. J. Siivola, J. Utriainen, M Linkoahe, G. Graeffe and T. Åberg, *Phys. Rev. Lett.* **32A**, 438 (1970).
14. P. Richard, J. Oltjen, K.A. Jamison, R.L. Kauffman, C.W. Woods and J.M. Hall, *Phys. Rev. Lett.* **54A**, 169 (1975).
15. F.S. Goulding and J.M. Jaklevic, *Am. Rev. Nucl. Sci.* **23**, 45 (1973).
16. F.S. Goulding and J.M. Jaklevic, *Nucl. Instrum. Methods* **142**, 323 (1977).
17. P. Van Espen and F. Adams, *X-Ray Spectrometry* **5**, 123 (1976).
18. P. Van Espen, L. Van't dack, F. Adams and R. Van Grieken, *Anal. Chem.* **51**, 961 (1979).
19. K. Das Gupta, *Phys. Rev. Lett.* **3**, 38 (1959).
20. P. Van Espen, H. Nullens and F. Adams, *Anal. Chem.* **51**, 1580 (1979).
21. P. Van Espen and F. Adams, *Anal. Chem.* **48**, 1823 (1976).
22. S.J.B. Reed and N.G. Ware, *J. Phys. E* **5**, 582 (1972).
23. P.J. Statham, *J. Phys. E* **9**, 1023 (1976).
24. J.S. Hansen, J.C. McGeorge, D. Nix, W.D. Schmidt-Att, I. Unus and R.W. Fink, *Nucl. Instrum. Methods* **106**, 365 (1973).
25. W.H. McMaster, M. Delgrande, J.H. Mallett and J.H. Hubbell, University of California, Lawrence Radiation Laboratory Report UCRL-50174 (1969).

Received 14 September 1979; accepted 14 October 1979